First-principles study of structural, electronic and optical properties of ZnF_2

Wu Jian-Bang(吴建邦), Cheng Xin-Lu(程新路)†, Zhang Hong(张 红), and Xiong Zheng-Wei(熊政伟)

Institute of Atomic and Molecular Physics, Sichuan University, Chengdu 610065, *China*

(Received 1 January 2014; revised manuscript received 2 April 2014; published online 22 May 2014)

The structural, electronic, and optical properties of rutile–, $CaCl_2$–, and PdF_2–ZnF_2 are calculated by the plane-wave pseudopotential method within the density functional theory. The calculated equilibrium lattice constants are in reasonable agreement with the available experimental and other calculated results. The band structures show that the rutile–, $CaCl_2$–, and PdF_2–ZnF_2 are all direct band insulator. The band gaps are 3.63, 3.62, and 3.36 eV, respectively. The contribution of the different bands was analyzed by the density of states. The Mulliken population analysis is performed. A mixture of covalent and weak ionic chemical bonding exists in ZnF_2. Furthermore, in order to understand the optical properties of ZnF_2, the dielectric function, absorption coefficient, refractive index, electronic energy loss spectroscopy, and optical reflectivity are also performed in the energy range from 0 to 30 eV. It is found that the main absorption parts locate in the UV region for ZnF_2. This is the first quantitative theoretical prediction of the electronic and optical properties of ZnF_2 compound, and it still awaits experimental confirmation.

Keywords: density functional theory, ZnF_2, electronic properties, optical properties

PACS: 71.15.Ap, 71.20.–b, 71.22.+i, 78.66.–w **DOI:** 10.1088/1674-1056/23/7/077102

1. Introduction

Fluorides have attracted significant attention due to their great potential applications in optical, mechanical, superconducting, and magnetic.[1–14] They are practically stable crystals in the atmosphere. As important inorganic functional materials, in the last decades, the fluorides with divalent metals AF_2 (A = Ca, Cd, Pb, Zn, Mn, Fe, Co, etc.) compounds have been extensively investigated because of their unique physical properties and possible applications in different fields. CaF_2 was used as a lens material for photolithographic applications at wavelengths in the deep ultraviolet region. This is due to its excellent transmission of vacuum ultraviolet light.[15,16] Meanwhile, CaF_2 may be converted into a semi-conducting material when doped with the elements of the III.[17] CdF_2 and PbF_2 are important scintillating materials that exhibit an electronic conductively behavior.[15,16] Similarly, CoF_2, MnF_2, and FeF_2 have gained extensive attention because of their excellent magnetic properties.[6–11]

ZnF_2 is an important optical and electronic conducting material. In 1950, it was reported by Crawford and Williams that rutile–ZnF_2 exhibits n-type electronic conduction, and its mobility and conductivity at room temperature are about 10 $cm^2/V{\cdot}s$ and 10^{-3} S/cm, respectively.[18] New synthesis routes for difluorides MF_2 (M = Fe, Mn, Zn, and Ni) were found by Pourroy *et al.*, and ZnF_2 is a rutile-type difluoride.[19] ZnF_2 thin films were deposited on SiO_2-glass and Al_2O_3-single crystal substrates by using the electron-beam evaporation. The ZnF_2 films show high orientation and crystallinity, and exhibit high transparency in the wave range from near-infrared to vacuum ultraviolet.[20] The amorphous ZnF_2, ZnF_2–BaF_2, AlF_3, and AlF_3–BaF_2 films were prepared on $CaF_2(111)$ substrates by an electron cyclotron resonance plasma-enhanced chemical vapor deposition technique. ZnF_2 films deposited on the substrates kept at 300 °C and 100 °C were crystalline and amorphous, respectively.[21] Chatterji *et al.* have investigated temperature dependence of the lattice parameters and the unit cell volume of ZnF_2 by neutron diffraction and have discovered negative thermal expansion (NTE) at low temperature.[22] Laser spectroscopy technique has been applied for studies of MnF_2 and ZnF_2 layers grown by molecular beam epitaxy on silicon substrates with the use of CaF_2 buffer layer. Quite complicated spectra of MnF_2:Sm and ZnF_2:Sm epitaxial films are observed at non-resonant excitation.[23] The core-hole effects on the theoretical fine structure of the X-ray absorption spectra of MgF_2 and ZnF_2 at F K-edge, the electronic and negative thermal expansion properties of ZnF_2 have been investigated by first-principles calculation. ZnF_2 is a direct band insulator with a bang gap of 3.65 eV, and this compound exhibits a negative thermal expansion at lower temperatures.[24,25] After doping by rare-earth atoms, ZnF_2 becomes an n-type semiconductor, and this material is attractive for applications as an efficient light emitter in the UV.[26] Recently, high-pressure and high-temperature behaviors of ZnF_2 with the rutile-type structure were investigated by using an energy-dispersive-type X-ray diffraction method. Two high-pressure phases were found in the range up to 15 GPa and 400 °C ($CaCl_2$– and PdF_2–

†Corresponding author. E-mail: chengxl@scu.edu.cn

© 2014 Chinese Physical Society and IOP Publishing Ltd

ZnF_2). The high-pressure behavior of ZnF_2 is similar to that of MgF_2.[27] The effect of high pressures up to 130 kbar on the structure of ZnF_2 at 25 and 300 °C was investigated by performing the X-ray diffraction in a chamber.[28] The high-pressure structural behavior of ZnF_2 has been studied by Raman spectroscopy and first-principles calculation. At ambient temperature and pressure, ZnF_2 is a rutile-type difluoride and its possible high-pressure phases are rutile, $CaCl_2$, and PdF_2 according to these experimental and calculated results.[14,29] However, to the best of our knowledge, there are no theoretical works that explore their optical properties. Hence, in order to interpret these experimental results and obtain a further understanding of rutile–, $CaCl_2$–, and PdF_2–ZnF_2, a theoretical investigation of the structural, electronic, and optical properties is necessary. In present work, the structural, electronic, and optical properties of rutile–, $CaCl_2$–, and PdF_2–ZnF_2 are calculated by performing the density functional theory (DFT) within the generalized gradient approximation (GGA).

This paper is organized as follows. The computational method is described in Section 2. The obtained results are presented and discussed in Section 3. Finally, the conclusions and remarks are given in Section 4.

2. Computational method

The calculation method we adopt is a plane-wave pseudopotential method based on density functional theory (DFT). The ultrasoft pseudopotential[30] is used with $2s^2 2p^5$ and $3d^{10}4s^2$ as the valence electron configuration for the fluorine and zinc atoms, respectively, to describe the electron–ion interaction. The exchange–correlation function is described by the generalized gradient approximation (GGA) in the scheme of Perdew–Burke–Ernzerhof (PBE).[31] The electron function was expanded in terms of plane-wave basis set with a cutoff energy of 480 eV. Reciprocal-space integration over the Brillouin zone was approximated through a careful sampling at finite number of k-points using a Monkhorst–Pack mesh.[32] The Brillouin-zone sampling mesh parameters for the k-point set were $8 \times 8 \times 10$, $8 \times 8 \times 10$, and $8 \times 8 \times 8$ for rutile–, $CaCl_2$–, and PdF_2–ZnF_2, respectively. To ensure the proper convergence of self-consistency calculation, the total energy was converged to less than 5.0×10^{-6} eV/atom. The crystal structures and the atom coordinates were fully relaxed without any restriction using the Broyden–Fletcher–Goldfarb–Shanno method[33] until the force on each atom converges to less than 0.01 eV/Å, stress below 0.02 GPa, and the displacement of atoms during the geometry optimization less than 5×10^{-4} Å. All the calculations were performed with the Cambridge Serial Total Energy Package (CASTEP) code,[34] at $T = 0$ K and $P = 0$ GPa.

3. Results and discussion

3.1. Structural parameters

At ambient temperature and pressure, ZnF_2 is a rutile-type difluoride and its possible high-pressure phases are rutile, $CaCl_2$, and PdF_2 according to experimental results.[29] For the rutile structure, the space group is $P4_2/mnm$ (136#), the site of Zn is $2a$ (0, 0, 0) and F is $4f$ (0.302, 0.302,0). For the $CaCl_2$ structure, the space group is $Pnnm$ (58#), the site of Zn is $2a$ (0, 0, 0) and F is $4g$ (0.275, 0.325,0). Similarly, for the PdF_2 structure, the space group is Pa-3 (205#), the site of Zn is $4a$ (0, 0, 0) and $8c$ (0.335, 0.335, 0.335). The models of the rutile–, $CaCl_2$–, and PdF_2–ZnF_2 are shown in Figs. 1(a)–1(c), respectively. A series of different constants of the rutile–, $CaCl_2$–, and PdF_2–ZnF_2 were set to calculate the total energy E and the corresponding primitive cell volume V, and a least-square fit of these energy–volume (E–V) data was made by the Brich–Burnaghan EOS.[35] The ground-state lattice constants and bulk modulus are listed in Table 1. It is indicated that our calculated results are in satisfactory agreement with the experimental and other calculated data.[14,20,22,25,27,28,36–38]

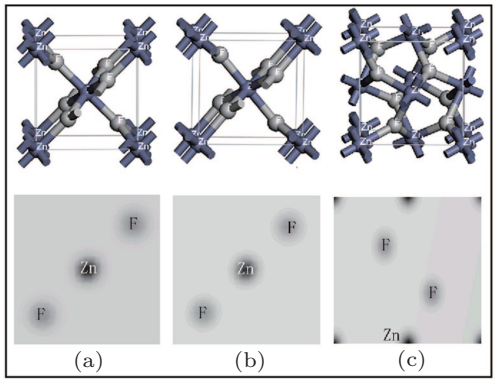


Fig. 1. (color online) Structures and charge densities of (a) rutile–, (b) $CaCl_2$–, and (c) PdF_2–ZnF_2.

3.2. Electronic properties

In order to analyze the optical properties of the rutile–, $CaCl_2$–, and PdF_2–ZnF_2, we firstly investigated their electronic properties based on the optimization. The band structure of rutile–ZnF_2 is shown in Fig. 2. The fermi level is chosen to coincide with the top of the valence band. The valence band maximum (VBM) and the conduction band minimum (CBM) occur at high symmetric G point, making this compound a direct band insulator. The band gap is about 3.63 eV, which is obviously less than the experimental values of 7.0–8.0 eV.[39] It is well known that the underestimated band gap can be attributed to the choice of exchange–correlation energy.[40] The band structure of $CaCl_2$–ZnF_2 is shown in Fig. 3. The $CaCl_2$–ZnF_2 is also a direct band insulator. The forbidden gap is about 3.62 eV at high symmetric G

Table 1. The lattice constants, band gaps, and bulk modulus of rutile–, $CaCl_2$–, and PdF_2–ZnF_2 at $T = 0$ K and $P = 0$ GPa.

Structure	a/Å	b/Å	c/Å	c/a	E_g/eV	B_0/GPa	Ref.
Rutile–ZnF_2	4.7123	4.7123	3.1791	0.6746	3.63	105.7	This work
	4.7534	4.7534	3.1943	0.6720	3.60	107.0	Cacl.[14]
	4.6637	4.6637	3.0919	0.6673	3.65	126.4	Cacl.[25]
	4.7034	4.7034	3.1335	0.6662	–	–	Expt.[36]
	4.7038	4.7038	3.1336	0.6662	–	–	Expt.[37]
	4.7048	4.7048	3.1336	0.6660	–	–	Expt.[20]
	4.7034	407034	3.1335	0.6662	–	–	Expt.[22]
	4.7140	4.7140	3.1320	0.6644	–	–	Expt.[27]
	4.7110	4.7110	3.1320	0.6648	–	–	Expt.[28]
	–	–	–	–	–	103.8	Expt.[38]
$CaCl_2$–ZnF_2	4.8004	4.8153	3.1801	0.6625	3.62	92.8	This work
	4.7872	4.7451	3.1734	0.6629	–	87.0	Cacl.[14]
	4.6120	4.7510	3.0650	0.6646	–	–	Expt.[27]
PdF_2–ZnF_2	5.1152	5.1152	5.1152	1.0000	3.36	111.1	This work
	5.0594	5.0594	5.0594	1.0000	–	116.0	Cacl.[14]
	4.8810	4.8810	4.8810	1.0000	–	–	Expt.[27]

point. It can be seen that the energy bands of the rutile– and $CaCl_2$–ZnF_2 are similar. This is due to the fact that the space group *Pnnm* is a subgroup of $P4_2/mnm$, and the symmetry of *Pnnm* is lower than the $P4_2/mnm$. The band structure of PdF_2–ZnF_2 is shown in Fig. 4. The band gap of the direct-band insulator PdF_2–ZnF_2 is about 3.36 eV. The important features of the band structure (main band gaps) for these compounds are given in Table 2. To further elucidate the nature of the electronic band structure, we also calculated the partial density of states (PDOS) of rutile–, $CaCl_2$–, and PaF_2–ZnF_2. For the rutile–ZnF_2 (Fig. 2), the valence band mainly consists of the 2s and 2p states of F, and 3d states of Zn. In the uppermost valence band, F 2p states are predominantly found between −6.50 and 0 eV, while F 2s states appear in the range from −22.26 to −19.72 eV. Zn 3d states are observed in the energy range from −6.50 to 0 eV. The conduction band mainly consists of the Zn 4s and 3p states. For the $CaCl_2$–ZnF_2 (Fig. 3), the valence band mainly arises from the 2s and 2p states of F, and 3d states of Zn. In the uppermost valence band, F 2p states are predominantly found between −6.71 and 0 eV, while F 2s states appear in the range from −22.53 to −19.39 eV. Zn 3d states are observed in the energy range from −6.71 to 0 eV. The conduction band mainly consists of the Zn 4s and 3p states. For the PdF_2–ZnF_2 (Fig. 4), the valence band mainly consists of the 2s and 2p states of F, and 3d states of Zn. In the uppermost valence band, F 2p states are predominantly found between −4.96 and 0 eV, while F 2s states appear in the range from −22.94 to −19.23 eV. Zn 3d states are observed in the energy range from −4.96 to 0 eV. The conduction band mainly consists of the Zn 4s and 3p states.

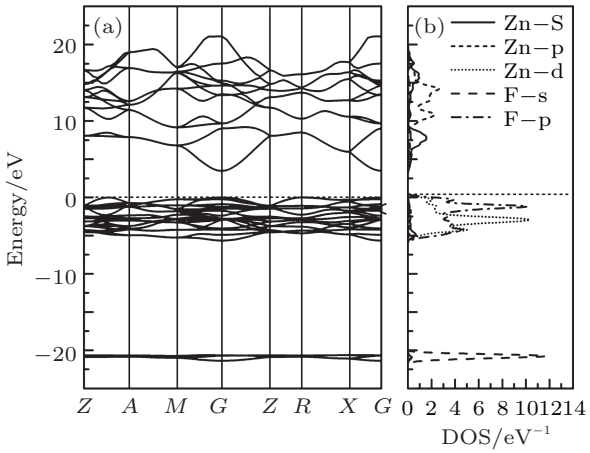


Fig. 2. (a) Band structure and (b) density of state of rutile–ZnF_2. The symmetry points of the first Brillouin zone: *G* (0, 0, 0), *Z* (0, 0, 1/2), *A* (1/2, 1/2, 1/2), *M* (1/2, 1/2, 0), *R* (0, 1/2, 1/2), and *X* (0, 1/2, 0).

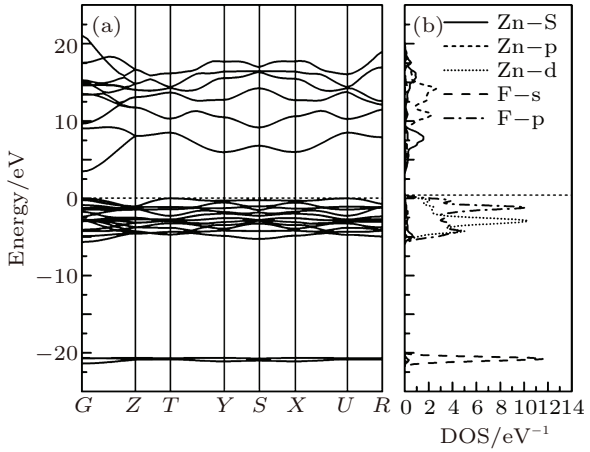


Fig. 3. (a) Band structure and (b) density of state of $CaCl_2$–ZnF_2. The symmetry points of the first Brillouin zone: *G* (0, 0, 0), *Z* (0, 0, 1/2), *T* (−1/2, 0, 1/2), *Y* (−1/2, 0, 0), *S* (−1/2, 1/2, 0), *X* (0, 1/2, 0), *U* (0, 1/2, 1/2), and *R* (−1/2, 1/2, 1/2).

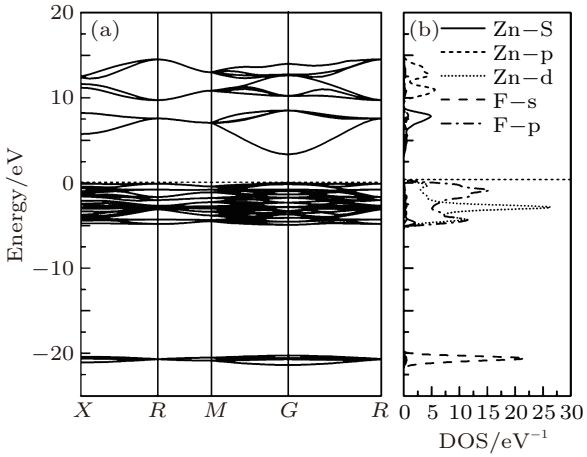


Fig. 4. (a) Band structure and (b) density of state of PdF_2–ZnF_2. The symmetry points of the first Brillouin zone: *G* (0, 0, 0), *X* (1/2, 0, 0), *M* (1/2, 1/2, 0), and *R* (1/2, 1/2, 1/2).

Table 2. Band gap energies E_g (eV) and symmetry of the valence-to-conduction band transition for rutile–, $CaCl_2$–, and PdF_2–ZnF_2.

Structure	E_g/eV		E_g/eV	
	$G \rightarrow$G	3.631	–	–
	$G \rightarrow Z$	8.104	$Z \rightarrow Z$	9.274
	$G \rightarrow A$	7.885	$A \rightarrow A$	8.616
rutile–ZnF_2	$G \rightarrow M$	6.890	$G \rightarrow M$	7.066
	$G \rightarrow R$	8.558	$R \rightarrow R$	8.563
	$G \rightarrow X$	6.012	$X \rightarrow X$	6.395
	$G \rightarrow$G	3.623	–	–
	$G \rightarrow Z$	8.085	$Z \rightarrow Z$	8.956
	$G \rightarrow T$	8.641	$T \rightarrow T$	8.648
$CaCl_2$–ZnF_2	$G \rightarrow Y$	6.095	$Y \rightarrow Y$	6.117
	$G \rightarrow S$	6.870	$S \rightarrow S$	7.068
	$G \rightarrow X$	5.875	$X \rightarrow X$	6.074
	$G \rightarrow U$	8.538	$U \rightarrow U$	8.538
	$G \rightarrow R$	8.085	$R \rightarrow R$	8.722
	$G \rightarrow G$	3.363	–	–
	$G \rightarrow X$	5.777	$X \rightarrow X$	5.771
PdF_2–ZnF_2	$G \rightarrow R$	7.568	$R \rightarrow R$	7.570
	$G \rightarrow M$	7.068	$M \rightarrow M$	7.454
	$G \rightarrow R$	7.674	$R \rightarrow R$	7.681

The Mulliken population analysis[41–43] is a good method to study bonding behavior and understand the charge transfer between the cation and anion. Our calculated results of population analysis are shown in Table 3. The positive value of charge represents the losing electron, and the negative represents the accepting electron. For the rutile– and $CaCl_2$–ZnF_2, the charge distributions are the same. The net charges of Zn and F atoms are 1.13 and −0.56 e, respectively. The charge transfer is from Zn to F, and the electron number of Zn 4s states is less than Zn 3p states. For the PdF_2–ZnF_2, the net charges of Zn and F atoms are 1.11 and −0.55 e, respectively. The charge transfer is also from Zn to F. It can be concluded that the Zn 4s states have stronger ability of losing electron compared with Zn 3p states. The charge density distributions that serve as a complementary tool to understand the electronic structure of the system have been studied. The charge density distributions along the (221) plane of rutile– and $CaCl_2$–ZnF_2 are shown in Figs. 1(a) and 1(b), and the charge density distribution along the (110) plane is shown in Fig. 1(c), and their 3D figures are shown in Fig. 5. The covalent character of any material can be related to the sharing of the charge between the cation and anion while the ionic character is related to the charge transfer between the cation and anion. The covalent character of ZnF_2 is due to the hybridization of Zn 3d with F 2p states between −6.71 and 0 eV. It can be seen that most of the charge is populated in the F–Zn bond direction, while the maximum charge resides on the F and Zn sites. We also performed the Mulliken overlap populations[41,44] of rutile–, $CaCl_2$–, and PdF_2–ZnF_2 to describe the interaction between atoms, as listed in Table 4. The positive overlap populations indicate the bonding between the atoms, while the negative represents anti-bonding, and the values denote the intensity of bonding. It is found that a mixture of covalent and weak ionic chemical bonding exists in ZnF_2.

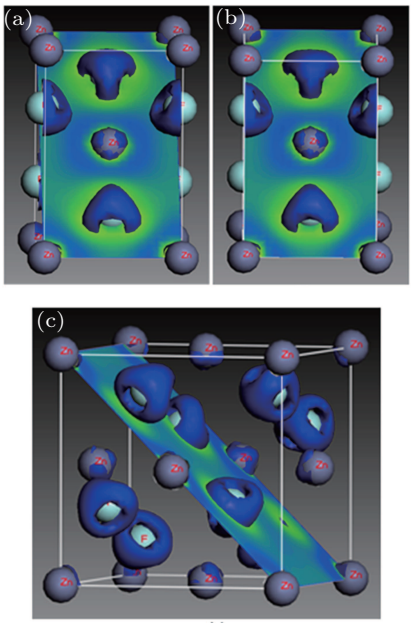


Fig. 5. (color online) Charge density distribution of ZnF_2 (3D) along the (221) plane for (a) rutile– and (b) $CaCl_2$–ZnF_2, and (c) along the (110) plane for PdF_2–ZnF_2.

Table 3. Mulliken population analysis of rutile–, $CaCl_2$–, and PdF_2–ZnF_2.

Structure	Species	s	p	d	Total	Charge/e
rutile–ZnF_2	F	1.95	5.61	0.00	7.56	−0.56
	Zn	0.36	0.51	10.00	10.87	1.13
$CaCl_2$–ZnF_2	F	1.95	5.61	0.00	7.56	−0.56
	Zn	0.36	0.51	10.00	10.87	1.13
PdF_2–ZnF_2	F	1.95	5.60	0.00	7.55	−0.55
	Zn	0.37	0.53	10.00	10.89	1.11

Table 4. Mulliken overlap populations of rutile–, $CaCl_2$–, and PdF_2–ZnF_2.

Structure	Bond	Population	Length/Å
rutile–ZnF_2	F–Zn	0.19	2.07022
	F–Zn	0.36	2.07264
	F–F	−0.04	2.65953
	F–F	−0.06	2.92944
$CaCl_2$–ZnF_2	F–Zn	0.19	2.06957
	F–Zn	0.36	2.07279
	F–F	−0.04	2.65979
	F–F	−0.06	2.93157
PdF_2–ZnF_2	F–Zn	0.18	2.08906
	F–F	−0.05	2.72080
	F–F	−0.01	2.82025

3.3. Optical properties

The complex dielectric function $\varepsilon(\omega) = \varepsilon_1(\omega) + \mathrm{i}\varepsilon_2(\omega)$ is known to describe the optical properties of materials. In this work, the excitonic effects are ignored while the local field effect is included under calculations. The imaginary part $\varepsilon_2(\omega)$ is calculated from the momentum matix elements between the occupied and unoccupied wave functions within the selection rules. Transitions between occupied and unoccupied states are caused by the photon absorption or emission. The real part $\varepsilon_1(\omega)$ of the complex dielectric function can be obtained using the Kramers–Kronig relationship. The imaginary part $\varepsilon_2(\omega)$ and real part $\varepsilon_1(\omega)$ of the dielectric function $\varepsilon(\omega)$ are given by[45–49]

$$\varepsilon_2(\omega) = \left(\frac{4\pi^2 e^2}{m^2\omega^2}\right)\sum_{i,j}\int_k \langle i|M|j\rangle^2 f_i(1-f_i) \times \delta\left(E_{j,k} - E_{i,k} - \omega\right)\mathrm{d}^3k, \quad (1)$$

$$\varepsilon_1(\omega) = 1 + \frac{2}{\pi}P\int_0^\infty \frac{\omega'\varepsilon_2(\omega')\,\mathrm{d}\omega'}{(\omega'^2 - \omega^2)}, \quad (2)$$

where e is the charge of free electrons, m is the mass of free electrons, ω is the frequency of incident photons, M is the dipole matrix, i and j are the initial and final states respectively, f_i is the Fermi distribution function for the i-th state, E_i is the energy of electron in the i-th state with crystal wave vector $\boldsymbol{k}$, and P denotes the principal value of the integral. Optical constants such as absorption coefficient $I(\omega)$, the refractive index $n(\omega)$, extinction coefficient $k(\omega)$, electron energy loss spectrum $L(\omega)$, and optical reflectivity $R(\omega)$ can be obtained. The concerned formulas are described as follows:[45–49]

$$I(\omega) = \sqrt{2}(\omega)\left[\sqrt{\varepsilon_1(\omega)^2 + \varepsilon_2(\omega)^2} - \varepsilon_1(\omega)\right]^{1/2}, \quad (3)$$

$$n(\omega) = \left[\frac{\sqrt{\varepsilon_1(\omega)^2 + \varepsilon_2(\omega)^2}}{2} + \frac{\varepsilon_1(\omega)}{2}\right]^{1/2}, \quad (4)$$

$$k(\omega) = \left[\frac{\sqrt{\varepsilon_1(\omega)^2 + \varepsilon_2(\omega)^2}}{2} - \frac{\varepsilon_1(\omega)}{2}\right]^{1/2}, \quad (5)$$

$$L(\omega) = \frac{\varepsilon_2(\omega)}{\varepsilon_1(\omega)^2 + \varepsilon_2(\omega)^2}, \quad (6)$$

$$R(\omega) = \left|\frac{\sqrt{\varepsilon(\omega)} - 1}{\sqrt{\varepsilon(\omega)} + 1}\right|^2. \quad (7)$$

The real and imaginary parts of the dielectric function are displayed in Figs. 6(a) and 6(b). From the real dielectric function $\varepsilon_1(\omega)$, the information about the electronic polarizability of the material can be obtained. The static dielectric constants at the zero frequency limit are obtained as $\varepsilon_1(0) = 2.20$, 2.20, and 2.14 for rutile–, $CaCl_2$–, and PdF_2–ZnF_2, respectively. For rutile– and $CaCl_2$–ZnF_2, one negative scale is found that the range is from 17.96 to 21.50 eV, and for PdF_2–ZnF_2, the range is from 13.88 to 17.00 eV. It indicates that the rutile–, $CaCl_2$–, and PdF_2–ZnF_2 show a metallic behavior in these frequency zones. In the curve of $\varepsilon_2(\omega)$, imaginary parts of the dielectric function for rutile– and $CaCl_2$–ZnF_2 are almost the same. Hence, there are four main peaks which are identified by the symbols A (1.40 at 7.79 eV), B (1.45 at 11.11 eV), C (1.85 at 15.64 eV) and D (1.81 at 16.83 eV) for rutile– and $CaCl_2$–ZnF_2. For the PdF_2–ZnF_2, three main peaks A′ (1.64 at 8.32 eV), B′ (2.00 at 10.91 eV), and C′ (2.04 at 13.16 eV) are observed. The peak A is mainly due to the transition from Zn 4s (7.82 eV) to the Zn 4s (15.64 eV) in the conduction band. The peak B may be due to the electronic transitions from Zn 3d (−4.24 eV) and F 2s (−4.27 eV) in the valence band to Zn 4s (7.83 eV) in the conduction. The peak C arises from the transitions: F 2p (−1.19 eV) to Zn 3p (14.22 eV). The peak D originates from the following transitions: F 2s (−20.78 eV) to Zn 3d (−4.24 eV). Similarly, the peak A′ is a significant contribution from F 2p (−1.49 eV) to Zn 4s (7.82 eV). The peak B′ emerges from Zn 3d (−2.86 eV) to Zn 4s (7.82 eV) and

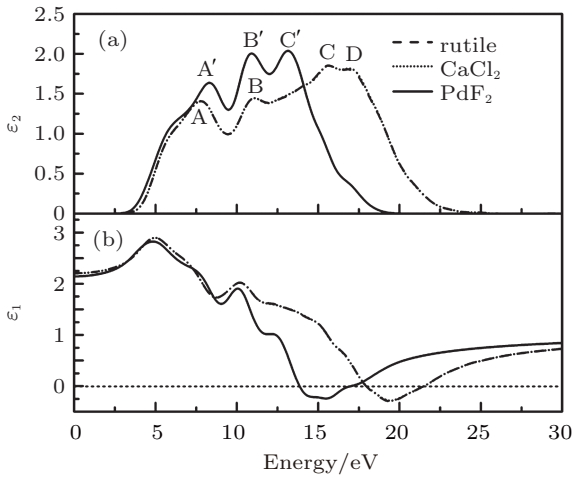


Fig. 6. The calculated (a) imaginary and (b) real parts of complex dielectric constant of rutile–, $CaCl_2$–, and PdF_2–ZnF_2.

peak C′ arises from the transitions: F 2p (at −1.49 eV) to Zn 3p (10.93 eV). The threshold energy of the dielectric function occurs at $E_0 = 3.52$, 3.52, and 3.36 eV for rutile–, $CaCl_2$–, and PdF_2–ZnF_2, which corresponds to the fundamental gap at equilibrium. It is well known that the materials with band gaps larger than 3.1 eV work well in the ultraviolet region of the spectrum.[50,51] Therefore, ZnF_2 will work excellently in the UV region as an optical material.

The optical absorption coefficients $I(\omega)$ of rutile–, $CaCl_2$–, and PdF_2–ZnF_2 are shown in Fig. 7. The absorption edge E_g can be obtained from the following relation:[52]

$$\alpha h\upsilon = C\left(h\upsilon - E_g\right)^n, \tag{8}$$

where $h\nu$ is the photon energy, C is a constant, and α is the optical absorption coefficient. We use a value of $n = 1/2$ for a direct band gap material and $n = 2$ for an indirect band gap material. Using the linear extrapolation method, the direct absorption edges with phonon absorption ($E_g^{dir} - E_{ph}$) are determined to be 6.48, 6.48, and 7.05 eV, respectively, for rutile–, $CaCl_2$–, and PdF_2–ZnF_2, where E_g^{dir} is the direct band gap, and E_{ph} the phonon energy. The absorption edge for rutile–ZnF_2 is consistent with Issei Suzuki's result (6.70 eV).[20] It shows that the absorption coefficients (inset) start from about 4.45, 4.45, and 4.43 eV, respectively, after which the intensities enhance with the increasing photon energy, and reach the maximum values of 2.55×10^5, 2.55×10^5, and 2.12×10^5 cm^{-1} (at 18.91, 18.91, and 14.03 eV), respectively. There is no electronic transition in the low energy range $E < 4.45$, 4.45, and 4.43 eV, respectively. The absorption region is quite wide, and the main absorption parts locate in the UV region.

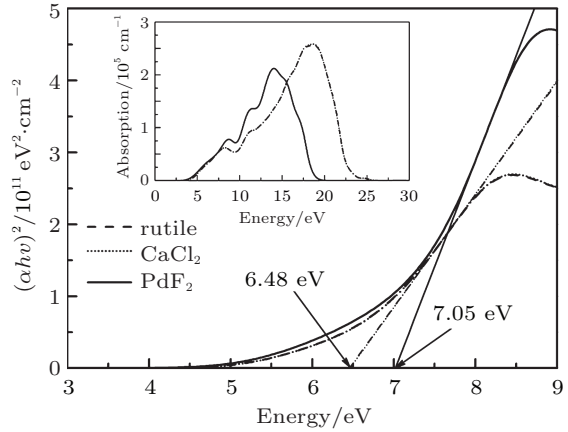


Fig. 7. Calculated optical absorption coefficient (inset) and variation of $(\alpha h\nu)^2$ as a function of photon energy for rutile–, $CaCl_2$–, and PdF_2–ZnF_2.

The calculated refractive index $n(\omega)$ and extinction coefficient $k(\omega)$ are depicted in Figs. 8(a)–8(c). The static refractive index $n(0)$, which implies the important quantity with a value of 1.48 for rutile–ZnF_2 equals the result for $CaCl_2$–ZnF_2. The static refractive index $n(0)$ of PdF_2–ZnF_2 is 1.46. The maximum refractive indices of rutile–, $CaCl_2$–, and PdF_2–ZnF_2 are 1.71, 1.71, and 1.69 (at 5.05, 5.05, and 4.98 eV), respectively. In the curve $k(\omega)$, the local maxima of the extinction coefficient $k(\omega)$ corresponds to the zero of $\varepsilon_1(\omega)$ ($\approx$ 17.72, 17.72, and 13.82 eV, for rutile–, $CaCl_2$–, and PdF_2–ZnF_2, respectively).

The calculated electron energy loss spectrum $L(\omega)$, and reflectivity $R(\omega)$ of the rutile–, $CaCl_2$–, and PdF_2–ZnF_2 are shown in Figs. 9(a) and 9(b). The loss function is an important parameter describing the energy loss of a fast electron traversing in a material. Generally, the peak of $L(\omega)$ spectrum represents the characteristic associated with the plasma resonance and the corresponding frequency is the so-called plasma frequency ω_p.[53] Figure 9(a) shows that the main peaks in energy loss spectrum $L(\omega)$ occur at 21.85, 21.85, and 17.78 eV for the rutile–, $CaCl_2$–, and PdF_2–ZnF_2, respectively. The reflectivity $R(\omega)$ is displayed in Fig. 9(b). Remarkably, the maximum in energy loss function $L(\omega)$ occurs while the real part of dielectric function $\varepsilon_1(\omega)$ drops below zero and the reflectivity starts decreasing rapidly (see Figs. 6(b) and 8).

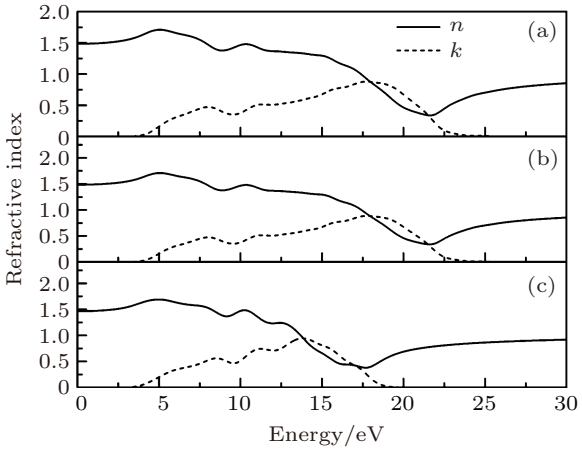


Fig. 8. Calculated refractive index $n(\omega)$ and the extinction coefficient $k(\omega)$ for (a) rutile–, (b) $CaCl_2$–, and (c) PdF_2–ZnF_2.

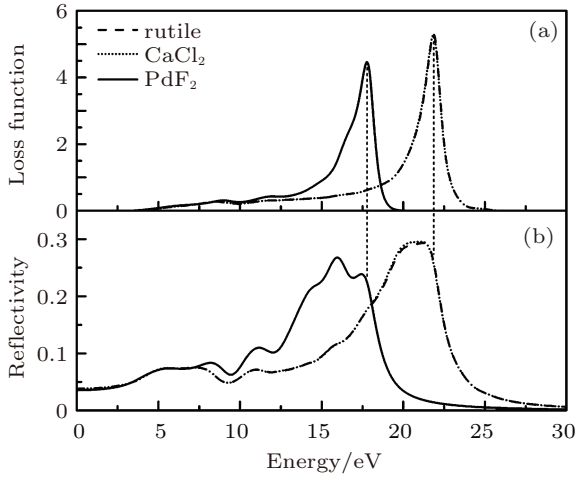


Fig. 9. Optical spectra as a function of photon energy for rutile–, $CaCl_2$–, and PdF_2–ZnF_2: (a) energy loss function and (b) reflectivity.

4. Conclusions

In summary, the structural, electronic and optical properties of the rutile–, $CaCl_2$–, and PdF_2–ZnF_2 have been calculated by performing the density functional theory (DFT) within the generalized gradient approximation (GGA). The calculated equilibrium lattice constants at zero pressure of these compounds are in reasonable agreement with the available experimental and other calculated results. The band structure calculations show that the rutile–, $CaCl_2$–, and PdF_2–ZnF_2 are all direct band insulators. The Mulliken population analysis shows that a mixture of covalent and weak ionic chemical bonding exists in ZnF_2. The dielectric function, absorption coefficient, refractive index, electronic energy loss spectroscopy, and optical reflectivity are also performed in the energy range from 0 to 30 eV. The main absorption part locates in the UV region for ZnF_2. Hence, ZnF_2 will work excellently in the UV region as an optical material.

References

[1] Singh G and Gallon T E 1984 *Solid State Commun.* **51** 281
[2] Babu K R, Lingam C B, Auluck S, Tewari S P and Vaitheeswaran G 2011 *J. Solid State Chem.* **184** 343
[3] Shirley E L, Terminello L J, Klepeis J E and Himsel F J 1996 *Phys. Rev. B* **53** 10296
[4] Eglitis R I, Shi H and Borstel G 2006 *Surf. Rev. Lett.* **13** 149
[5] Letz M, Gottwald A, Richter M and Parthier L 2009 *Phys. Rev. B* **79** 195112
[6] Martel P, Cowley R A and Stevenson R W H 1968 *J. Appl. Phys.* **39** 1116
[7] Zavrazhnaya E M and Chepurnykh G K 2008 *Phys. Solid State* **50** 882
[8] Lines M E 1965 *Phys. Rev.* **137** A982
[9] Wertheim G K, Guggenheim H J and Buchanan D N E 1969 *J. Appl. Phys.* **40** 1319
[10] Moriya T, Motizuki K, Kanamori J and Nagamiya T 1956 *J. Phys. Soc. Jpn.* **11** 211
[11] Ramos C A, Lederman D, King A R and Jaccarino V 1990 *Phys. Rev. Lett.* **65** 2913
[12] Khosla R P 1969 *Phys. Rev.* **183** 696
[13] Lee B C, Khilko A Y, Shusterman Y V, Yakovlev L, Sokolov N S and Kyutt R N 1998 *Appl. Surf. Sci.* **123** 590
[14] Wu X and Wu Z 2006 *Eur. Phys. J. B* **50** 521
[15] Samara G A 1979 *J. Phys. Chem. Solid.* **40** 509
[16] Derenzo S E, Moses W W, Cahoon J L, Perera R C C and Litton J E 1990 *IEEE Trans. Nucl. Sci.* **37** 203
[17] Ritus A I, Pronin A V, Volkov A A, Lunkenheimer P, Loidl A, Shcheulin A S and Ryskin A I 2002 *Phys. Rev. B* **65** 5209
[18] Crawford Jr. J H and Williams F E 1950 *J. Chem. Phys.* **18** 775
[19] Pourroy G and Poix P 1989 *J. Fluorine Chem.* **42** 257
[20] Suzuki I, Omata T, Shiratsuchi Y, Nakatani R, Kitamura N and Otsuka-Yao-Matsuo S 2013 *Thin Solid Films* **534** 508
[21] Masanori S, Shuhei T, Miyuki T, Akio K and Yoji K 2001 *J. Non-Cryst. Solid.* **284** 153
[22] Tapan C, Mohamed Z and Thomas C H 2011 *Appl. Phys. Lett.* **98** 181911
[23] Gastev S V, Hoffman K R, Kaveev A K, Reeves R J and Sokolov N S 2004 *J. Cryst. Growth* **268** 536
[24] Yamamoto T, Mizoguchi T, Tatsumi K, Tanaka I, Adachi H, Muramatsu Y, Gullikson E M and Perera R C C 2004 *Mater. Trans.* **45** 1991
[25] Wang L, Yuan P F, Wang F, Sun Q, Liang E J and Jia Y 2012 *Mater. Res. Bull.* **47** 1113
[26] Senda T, Cho Y, Hirakawa T, Okamoto H, Takakura H and Hamakawa Y 2000 *Jpn. J. Appl. Phys.* **39** 4716
[27] Keiji K and Takumi K 2008 *Solid State Commun.* **145** 279
[28] Kabalkina S S, Vereshchagin A L F and Lityagina L M 1968 *Sov. Phys.-Dokl.* **12** 946
[29] Perakis A, Lampakis D, Boulmetis Y C and Raptis C 2005 *Phys. Rev. B* **72** 144108
[30] Milman V, Winkler B, White J A, Packard C J, Payne M C, Akhmatskaya E V and Nobes R H 2000 *Int. J. Quantum Chem.* **77** 985
[31] Perdew J P, Burke K and Ernzerhof M 1996 *Phys. Rev. Lett.* **77** 3865
[32] Monkhorst H J and Pack J D 1976 *Phys. Rev. B* **13** 5188
[33] Pfrommer B G, Cote M, Louie S G and Cohen M L 1997 *J. Comput. Phys.* **131** 233
[34] Segall M D, Lindan P J D, Probert M J, Pickard C J, Hasnip P J, Clark S J and Payne M C 2002 *J. Phys. Condens. Matter* **14** 2717
[35] Murnaghan F D 1944 *Proc. Natl. Acad. Sci. USA* **30** 244
[36] Hao Y, Gao Y, Wang B, Qu J, Li Y, Hu J and Deng J 2001 *Appl. Phys. Lett.* **78** 3277
[37] O'Toole N J and Streltsov V A 2001 *Acta Cryst. B* **57** 128
[38] Gerlich D, Hart S and Whittal D 1984 *Phys. Rev. B* **29** 2142
[39] Nakanishi Y, Naito S, Nakamura T, Hatanaka Y and Shimaoka G 1996 *Appl. Surf. Sci.* **92** 400
[40] Zhang X D, Guo M L, Liu C L, Li W X and Hong X F 2008 *Appl. Phys. Lett.* **93** 012103
[41] Mulliken R S 1955 *J. Chem. Phys.* **23** 1833
[42] Segall M D, Pickard C J and Shah R 1996 *Mol. Phys.* **89** 571
[43] Yun J N, Zhang Z Y, Yan J F and Deng Z H 2010 *Chin. Phys. B* **19** 017101
[44] Segall M D, Shah R and Pickard C J 1996 *Phys. Rev. B* **54** 16317
[45] Ambrosch D C and Sofo J O 2006 *Comput. Phys. Commun.* **175** 1
[46] Fox M 2001 *Optical Properties of Solids* (New York: Oxford University Press)
[47] Wooten F 1972 *Optical Properties of Solids* (New York: Acadmic) p. 179
[48] Yao G, Chen Y, An X Y, Jiang Z Q, Cao L H, Wu W D and Zhao Y 2013 *Chin. Phys. Lett.* **30** 067101
[49] Lü B, Zhou X, Linghu R F, Wang X L and Yang X D 2011 *Chin. Phys. B* **20** 036104
[50] Maqbool M, Amin B and Ahmed I 2009 *J. Opt. Soc. Am. B* **26** 2181
[51] Maqbool M and Kordesch M E 2009 *J Opt Soc Am B* **26** 998
[52] Srikant V and Clarkea D R 1997 *J. Appl. Phys.* **81** 6357
[53] Anderson O L 1963 *J. Phys. Chem. Solid* **24** 909